TISSUE ENGINEERING: Part A
Volume 14, Number 7, 2008

DOI: 10.1089/ten.tea.2007.0186

Image-Guided Tissue Engineering of Anatomically Shaped Implants via MRI and Micro-CT Using Injection Molding

JEFFERY J. BALLYNS, B.S.,[1,2] JASON P. GLEGHORN, Ph.D.,[1,2] VICKI NIEBRZYDOWSKI, B.S.,[1] JEREMY J. RAWLINSON, Ph.D.,[1] HOLLIS G. POTTER, M.D.,[3] SUZANNE A. MAHER, Ph.D.,[3] TIMOTHY M. WRIGHT, Ph.D.,[3] and LAWRENCE J. BONASSAR, Ph.D.[1,2]

ABSTRACT

This study demonstrates for the first time the development of engineered tissues based on anatomic geometries derived from widely used medical imaging modalities such as computed tomography (CT) and magnetic resonance imaging (MRI). Computer-aided design and tissue injection molding techniques have demonstrated the ability to generate living implants of complex geometry. Due to its complex geometry, the meniscus of the knee was used as an example of this technique's capabilities. MRI and microcomputed tomography (μCT) were used to design custom-printed molds that enabled the generation of anatomically shaped constructs that retained shape throughout 8 weeks of culture. Engineered constructs showed progressive tissue formation indicated by increases in extracellular matrix content and mechanical properties. The paradigm of interfacing tissue injection molding technology can be applied to other medical imaging techniques that render 3D models of anatomy, demonstrating the potential to apply the current technique to engineering of many tissues and organs.

INTRODUCTION

A MAJOR ADVANTAGE to tissue engineering technologies is that they enable the generation of tissue in specific shapes. Shape generation is critical for craniofacial[1] and plastic surgery[2] applications as well as orthopedic applications[3,4] where joint conformity is required. Efforts to engineer tissue in anatomic shapes have shown promise, including forming cartilage into the shape of a human ear,[5] injecting periosteal cells into porous coral in the shape of a distal phalanx for thumb reconstruction,[6] generating a bone–cartilage composite shaped as a human mandibular joint,[7] creating anatomically shaped patellar articular cartilage using stereophotogrammetry data,[8] and forming phalanges and small joints through selective placement of bone and cartilage cells into a biodegradable synthetic polymer scaffold.[9] Recurring challenges in these methods include the accuracy, speed, and reproducibility of the process by which these implants are made. For example, methods to create anatomic geometries by molding polyglycolic acid (PGA) or polylactic acid (PLA)[5,10] or carving of ceramic implants[6] require extensive time for implant fabrication, and separate procedures for cell seeding are inefficient. Other procedures involving 3D printing of anatomically shaped scaffolds have faced similar challenges in efficiently localizing cells on the scaffolds.[11] No method currently exists for rapidly incorporating patient-specific geometry into tissue-engineered implants.

Injection molding techniques could provide an innovative approach to generating implants of complex geometry in a much shorter time.[12,13] Previous work showed that computer-aided design (CAD) can be combined with tissue injection molding technologies to fabricate very small, precise, cell-seeded alginate structures that maintain

[1]Mechanical and Aerospace Engineering, Cornell University, Ithaca, New York.
[2]Biomedical Engineering, Cornell University, Ithaca, New York.
[3]Department of Biomechanics, Hospital for Special Surgery, New York, New York.

shape fidelity throughout *in vitro* culture.[14] CAD-based techniques have also been applied to casting osteochondral constructs with conformal joint surfaces.[8] However, no study has yet demonstrated an ability to produce cell-seeded geometries derived from clinically used imaging modalities.

The goal of this study was to apply CAD tissue injection molding techniques to engineer a whole meniscus. Medically, injuries to the meniscus pose a relevant clinical problem with over 750,000 meniscal surgeries conducted each year, the most common treatment for which is partial or total removal of the injured tissue (i.e., meniscectomy).[4] Current meniscal tissue engineering efforts have focused on developing repair methods through the use of mesenchymal stem cells[15] to address point defects and using scaffolding materials such as a collagen-based meniscus implant[16,17] to aid in regeneration of complex tears and defects. The concept of using fibrochondrocyte-seeded scaffolds for generation of meniscal tissue has been demonstrated with several scaffolding materials, including agarose gels,[18] nonwoven PGA meshes,[18] and polyethylene terephthalate scaffolds.[19] Further, exposing these constructs to different growth factors[20] and media mixing culture conditions[18,19] has been used to stimulate meniscus tissue growth.

Cadaveric meniscal allografts are clinically used, but this method of treatment suffers due to the scarcity of donor tissue, difficulties in matching the native joint architecture, and the risk of disease transmission. Matching the size of the native meniscus is of particular importance to ensure the appropriate distribution of pressure across the joint. Image-guided echo time of the meniscus addresses the existing issues associated with meniscal allografts. There have been very few studies that attempt to engineer whole menisci,[21,22] which could be due to the large size of these constructs and difficulty in replicating its complex geometry.

The current research focuses on the incorporation of standard medical imaging tools, specifically magnetic resonance imaging (MRI) and computed tomography (CT; specifically for the current work, microcomputed tomography, or μCT), to design templates for tissue-engineered implants. Both of these imaging methods are commonly used for diagnosis and monitoring of tissue disease, and thus could be easily incorporated into the process of designing therapies. While MRI is commonly used for diagnosis of soft tissue injuries, issues of resolution and thresholding are challenging in delineating the meniscus from adjacent soft tissue. In contrast, CT/μCT is not typically used for soft tissue imaging, but had necessary resolution to facilitate tissue delineation. To test the feasibility of using MRI and μCT imaging data for tissue engineering, an injection molding system was designed based on these imaging modalities, and constructs generated by this technique were cultured for 8 weeks and monitored by gross shape inspection, assessment of compressive mechanical properties, quantification of biochemical composition, and analysis of ECM localization by histology.

MATERIALS AND METHODS

Imaging

Magnetic resonance imaging of five skeletally mature sheep knees (donated by Dr. Simon Turner, Colorado State University) was performed on a clinical 3T MR unit (Twin Speed; General Electric Health Care, Milwaukee, WI) using a commercially available, eight-channel, receive-only knee coil (*In Vivo*, Milwaukee, WI). Sagittal fast spin echo (FSE) sequences were acquired with a repetition time (TR) of 4800 ms, echo time (TE) of 26.8 ms (effective), echo train length of 12, field of view of 13 cm, matrix of 512×416, and slice thickness of 2.0 mm with no gap, resulting in a spatial resolution of 253.9 μm (frequency)×312.5 μm (phase)× 1 mm, at three excitations. Phase direction was superior to inferior, and receiver bandwidth was 62.5 kHz over the entire frequency range.

In addition, sagittal 3D spoiled gradient echo (SPGR) sequences were acquired with selective water excitation, using a flip angle of 10°, TR of 16.8 ms, TE of 4.1 ms, field of view of 13 cm, matrix of 512×512, and slice thickness of 0.5 mm with no gap, resulting in a spatial resolution of 253.9 μm (frequency)×253.9 μm (phase)×0.5 mm at one excitation. Receiver bandwidth was again 62.5 kHz over the entire frequency range.

The medial meniscus from each knee was dissected, soaked in Omnipaque® Iohexol (GE Healthcare, Inc., Princeton, NJ) 300 mg I/mL contrasting agent for 2 h, and μCT scanned using an Enhanced Vision Systems Model Ms-8 *In Vitro* Micro-CT Scanner (GE Healthcare, formerly EVS, Ontario, Canada). The scans were taken using short scan X-ray settings of 70 kV, 90 mA, 3000 ms exposure time, with 400 views, and 0.023 mm/pixel resolution. Scans were calibrated using values for bone, air, and saline. Sheep menisci were the largest animal menisci that would fit into the μCT core, and were thus used for both imaging modalities.

Mold design

MRI data sets in DICOM format were viewed and manually segmented for isolation of the meniscal area (Fig. 1, step 1). Isolated meniscal segments from DICOM files were used to render a 3D representation in a point cloud image (sliceOmatic v4.3; TomoVision, Montreal, Canada). Conversion of the point cloud image to a surface image allowed for formatting and generation of a solid model (Studio 4.0; Geomagic Inc., Research Triangle Park, NC). The meniscus was then ready to be imported into CAD and be employed for mold design.

The μCT scan was visualized as a surface image (MicroView; GE Healthcare Inc., Princeton, NJ) and exported for processing and file conversion. Upon conversion to a solid representation (Geomagic Studio 4.0), the image was used for mold design in CAD (SolidWorks Educational Edition) or converted to an STL file to 3D print an ABS plastic replica

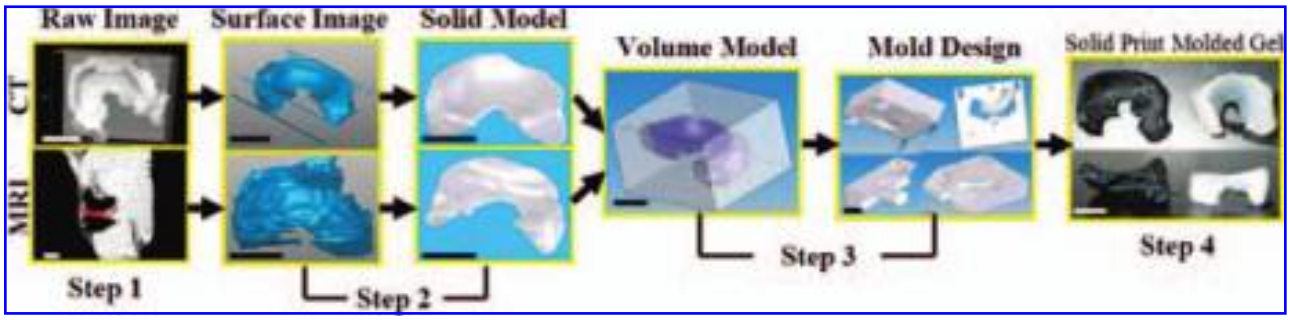

FIG. 1. Image processing steps for CT and MRI scans of an ovine meniscus being converted from its raw form to a surface image (step 1), then cleaned and converted to a solid model (step 2), and imported into CAD software for mold design (step 3). The embedded meniscus generated a suitable mold that achieved good shape fidelity as compared with the solid printed model (step 4). Scale bar = 10 μm. Color images available online at www.liebertpub.com/ten.

of the tissue on a fused deposition modeling platform or FDM 3000 machine (Stratasys, Eden Prairie, MN).

The CAD mold design process was identical for both μCT and MRI (Fig. 1). The image of the solid meniscus was embedded into a block and served as a virtual negative for the mold. The block was divided into four sections that allowed for removal of intact meniscus constructs from the mold. Molds were printed using an FDM 3000 machine.

Injection molding

Using previously developed methods,[12] the meniscus was removed intact from 1- to 3-day-old bovine knee joints (Gold Medal Packing, Oriskany, NY) and diced into 1 mm^3 cubes. Bovine cells were used instead of sheep cells because they were the most readily available and consistent cell source. The tissue was digested overnight in 0.3% collagenase, 100 μg/mL penicillin, and 100 μg/mL streptomycin in Dulbecco's modified Eagle's medium (DMEM) (Gibco-Invitrogen, Grand Island, NY). The following day the cells were washed, isolated, and counted. Viability ranged between 82% and 87%. To generate the 50 molded constructs in this study, cells from 52 menisci and 16 animals were harvested. The 50 constructs were produced in 9 batches with each batch containing cells pooled from 1 to 2 animals and 4 to 8 menisci. The engineered constructs made from these nine batches were distributed randomly across time points.

Cells were then seeded at 50 million cells/mL in 2% LVG alginate (FMC Biopolymer, Drammen, Norway), mixed with $CaSO_4$ (Sigma–Aldrich, St. Louis, MO) at 0.02 g/mL to crosslink the alginate, and injected into meniscus molds. This cell seeding density was chosen based on prior studies using injection molding technology to deliver articular chondrocytes. The current cell seeding density was optimal for tissue growth in articular chondrocytes.[12–14,23] The alginate remained in the mold for 20 min to allow for sufficient crosslinking before removing the gel structure from the mold. Average molded construct size was 25.3×17.4×6.6 mm (length from the outside of each horn×average width from the front of the horn to the back of construct×height). Samples were placed into static culture for up to 8 weeks in culture media composed of DMEM, with 10% FBS, 100 μg/mL penicillin, and 100 μg/mL streptomycin.

Biochemistry

Native and engineered samples harvested at 0, 1, 2, 4, 6, and 8 weeks were photographed, cut into cross sections, and photographed again. Six-millimeter-diameter by 1-mm-thick discs were biopsied from cultured menisci and from native tissue. The discs were cored from similar locations in both engineered and native tissues, and used for biochemical analysis or mechanical testing. Other cross sections were fixed for histology. Samples reserved for biochemical analysis were weighed, frozen, lyophilized, and weighed again. Lyophilized discs were digested in 1.25 mg/mL papain solution overnight at 60°C.[24] Papain digests of tissue-engineered constructs and native controls were analyzed for DNA content via Hoechst DNA assay,[25] glycosaminaglycans (GAG) through a modified DMMB spectrophotometric assay done at pH 1.5,[26] and collagen content via hydroxyproline assay.[27] Nine samples per meniscus were gathered for biochemical analysis of extracellular matrix (ECM) composition.

Histology

Cross sections of molded constructs were fixed in 10% buffered formalin with 1 mM $CaCl_2$ to prevent gel solubilization.[28] Fixed sections were then stained with Safranin-O at pH 2.0 to observe GAG formation. Sections were then stained with picrosirius red to observe collagen formation.

Mechanical testing

Discs (6 mm diameter, 1 mm thick) were tested in confined compression to determine the equilibrium modulus (EnduraTech; Electroforce (ELF) 3200 System, Minnetonka, MN). As described previously,[12] stress relaxation tests were performed by imposing 10 steps of 50 μm on the gels and native controls with resultant loads fit to a poroelastic model to calculate the equilibrium modulus.

Statistical analysis

Data were analyzed by one-way ANOVA to detect differences in aggregate modulus, GAG, collagen, and DNA content over time using $p < 0.05$ as a threshold of statistical significance. Time points that were found to be significantly different were then further analyzed through *post hoc* comparisons with the Bonferroni correction. All statistical analyses were implemented with Sigmastat version 3.0 (SYSTAT, San Jose, CA), and all data expressed as mean ± SEM.

RESULTS

Inspection of cross sections demonstrated increases in opacity of the construct with time in culture, indicative of ECM deposition. This matrix deposition was heterogeneous with more pronounced opacity in the center. Gross inspection of MRI- and μCT-generated models (Fig. 1, step 4) indicate that both imaging modalities can serve as a template for mold design. While the μCT model has excellent surface resolution compared to MRI, MRI imaging produced anatomically similar geometries with superior fibrocartilage–bone contrast. There were no significant differences between samples made by MRI and μCT (data not shown). Samples shown are representative of both. Anatomically shaped constructs retained shape for the duration of culture with ~87% (33/38) remaining as intact constructs (Fig. 2A). Although quantitative volume measurements were not taken, gross inspection did not reveal any changes in size. Whole construct weights were not measured due to fragility of constructs at early times.

Safranin-O staining of engineered tissue cross sections demonstrated progressive proteoglycan deposition, with spatial patterns of staining that were consistent with observations of opacity from gross inspection of cross sections (Fig. 2B, C). Picrosirius red staining of sections from the molded constructs revealed progressive deposition and orientation of collagen across 8 weeks of culture (Fig. 2D), trending toward the highly organized matrix of native meniscus.

Progressive tissue formation, as indicated by the accumulation of ECM, occurred throughout the entire culture

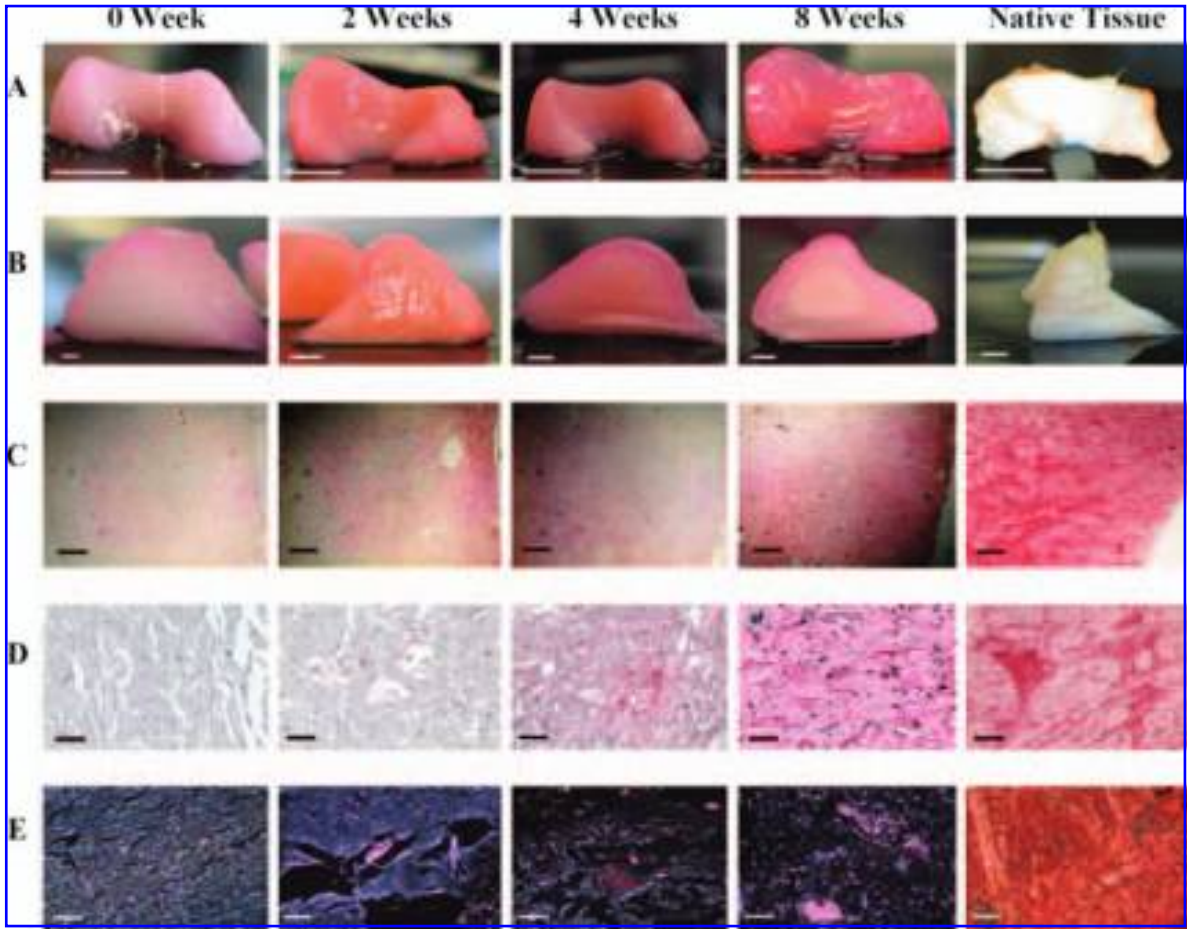

FIG. 2. Photographs of (**A**) intact implants, (**B**) cross-sectional views, (**C**) tissue sections stained with Safranin-O at 40× original magnification, (**D**) tissue sections stained with Safranin-O at 200× original magnification, and (**E**) tissue sections stained with picrosirius red at 200× original magnification for engineered cartilage at 0, 2, 4, or 8 weeks and native meniscal tissue. Scale bars represent (**A**) 10 mm, (**B**) 2 mm, (**C**) 500 μm, and (**D, E**) 100 μm. Color images available online at www.liebertpub.com/ten.

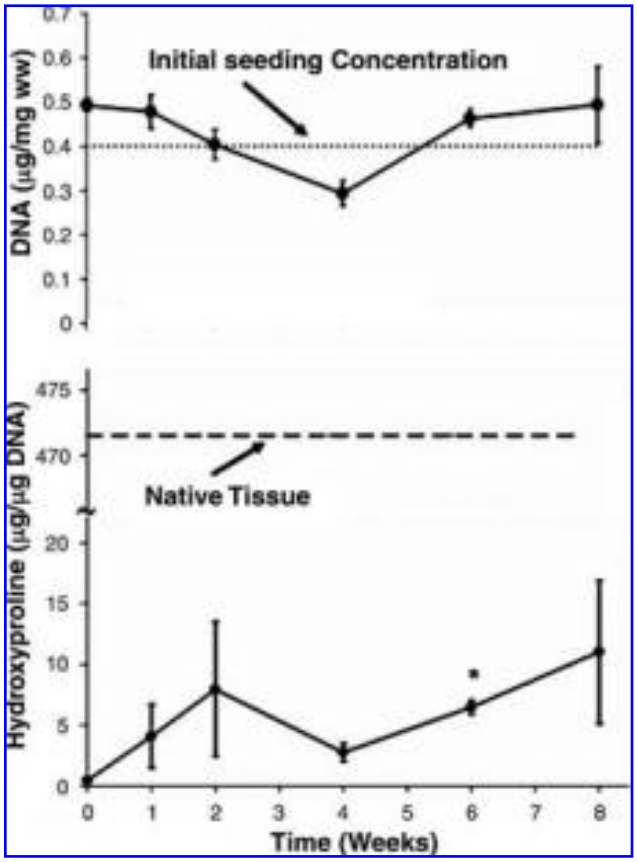

FIG. 3. Temporal changes in DNA content and hydroxyproline content in tissue-engineered menisci and native meniscus. Data represent mean ± SEM for $n = 5$–8 samples.

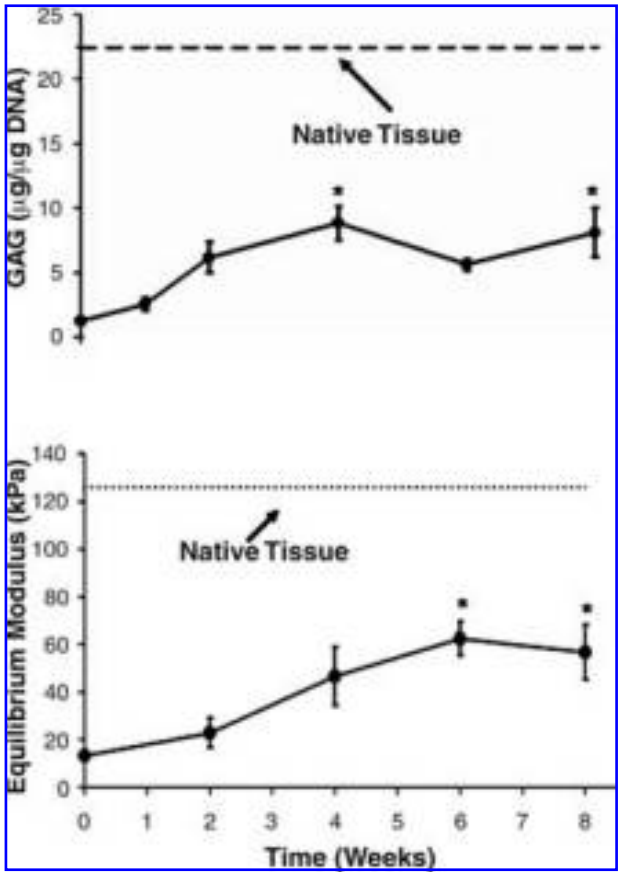

FIG. 4. Temporal changes in GAG content and compressive equilibrium modulus in tissue-engineered menisci and native meniscus. Data represent mean ± SEM for $n = 5$–8 samples.

period. Cell density as indicated by DNA content did not vary with time (Fig. 3) and remained within 25% of the initial seeding density. Collagen content indicated by hydroxyproline content (Fig. 3) increased significantly up to 6 weeks ($p < 0.05$). At 8 weeks, engineered tissue containing approximately 2.3% of the collagen found in tested native tissue controls normalized to DNA. At 4 and 8 weeks, a significant increase in GAG content ($p < 0.05$) occurred, reaching 36% that of native tissue controls. The equilibrium modulus in the engineered menisci reached 50% of the native tissue controls at 6 weeks and showed significant increases in modulus at 6 ($p < 0.01$) and 8 weeks ($p < 0.05$) (Fig. 4). Tests of native tissue controls yielded values for hydroxyproline content,[28,29] GAG content,[29,30] and equilibrium modulus[29,31,32] similar to those reported previously.

DISCUSSION

This study established the design of an injection molding system based on medical imaging data to produce tissue-engineered constructs that reproduced the geometric properties of native tissue. Injection-molded samples retained geometry over 8 weeks in culture. The few constructs that did fail did so due to tears formed when removing constructs from molds, which propagated when being moved in and out of the incubator for media changes. Progressive tissue formation was demonstrated by monotonic increases in ECM content and mechanical properties. After 8 weeks, the compressive modulus of engineered tissue was ~ 50% that of native meniscus. These results demonstrate the ability to use patient-specific geometry to rapidly engineer tissue, a feature unavailable in other current tissue engineering methods.

GAG and collagen contents after 8 weeks were similar to other studies.[18–21] Unlike culture studies of meniscal fibrochondrocytes in agarose gels,[19] no significant cell loss or cell death was observed. DNA content did not significantly change over the course of this study, consistent with previous studies documenting delivery of articular chondrocytes by injection molding in alginate.[12,14] Further, cell distribution was uniform throughout culture, suggesting that there were no regions of central necrosis even in these relatively large samples (Fig. 2). In contrast to other studies, ECM loss did not occur at later time points as seen in PGA meshes.[19] The continuing problem remains in the ability to generate mechanically equivalent tissues to that of a native meniscus.[19,21,22] Upregulating collagen production could provide

increased mechanical stability and aid in decreasing GAG loss to the surrounding media.[19] The confined compression modulus determined in the current study is thought to relate primarily to GAG content.[33,34] Indeed, the GAG/DNA has 36% of native meniscus, and equilibrium modulus was 50% of native. Clearly, collagen content was lower, but this would likely be reflected in other testing geometries such as tension or shear, which are not reported here. No ascorbic acid was added to the culture medium in this study, which could explain why collagen content was low. Studies that have implanted engineered meniscal scaffolds into an animal model[21,22] have had varying results, all of which suffer from a mismatch of mechanical properties and accurate geometry. Application of the technologies presented in this study could aid in the process of guiding meniscal constructs to reach their proper mechanical function.

Unlike the studies described above, the current experiments focused on reproducing meniscal geometry with tissue-engineered meniscus. A consequence of this approach is the development of spatial gradients within tissue constructs with time in culture. Gross morphology and histology show inhomogeneities in ECM accumulation with more tissue localized in the center. Even though our engineered constructs were relatively large in size compared to other studies,[18–20] this is inconsistent with central necrosis or nutrient deposition. The preferential accumulation of ECM in the center of these constructs could be due to a lack of ECM loss to the media compared to the surface. The centers of these constructs were probably hypoxic, and previous studies show that low O_2 enhances ECM formation for articular chondrocytes[35] as well as meniscal fibrochondrocytes.[36] Future studies will characterize spatial and directional properties in these samples to understand the effects of heterogenous matrix accumulation in engineered 3D anatomical structures.

While the process of generating anatomically shaped cell-seeded menisci does appear to be manpower heavy, the total time from start to finish was approximately 10 h, half of which was for image processing. Production time can be greatly reduced by auto-segmentation algorithms to extract data from MRI images, improved editing functions to aid in formatting and conversion to a solid model, and automated algorithms for mold design in CAD software. However, even with the current system described here, clinical deployment time between imaging for diagnosis and surgical therapy would likely be days to weeks, which would be adequate time to design an implant.

The success of image-based injection molding in medicine relies on integrating the use of clinically relevant field strength MRI and other accepted imaging techniques. Further, through use of diffusion tensor imaging, the ability to map orientation through fractional anisotropic mapping and microstructural features of soft tissues[37] may make MRI the preferred modality for design and assessment of structures such as meniscus. μCT is typically used to image dense tissue, but was used in this study to obtain a high-resolution template for construct generation. While MRI imaging would more likely be used in a clinical setting, it is possible that μCT could be used. Palmer *et al.*[38] have established a technique to visualize articular cartilage *in vitro* with μCT with contrast agents that may be used *in vivo*.

Obtaining high geometric fidelity can be of great importance, especially for the meniscus where a deviation by more than 10% in meniscal size matching[39] can result in detrimental loads across the joint. Due to the complex geometry of the meniscus, correct size matching to restore normal contact pressure is no trivial task. Current efforts are being made to denote the critical geometric parameters of the meniscus[40] as well as improve the allograft matching process.[41] Lastly, efforts are being made to quantify geometric accuracy of injection molds compared to native tissue. Geometric quantification will also aid in tracking shape fidelity over culture time.

The interface of tissue injection molding technology is not limited to μCT and MRI, but can be applied to any other medical imaging technique that has the ability to render a 3D model, including angiography, fluoroscopy, mammography, and ultrasound. Similarly, the injection molding technique presented here is not limited to the use of alginate as a scaffold material and could be adopted for use with other common tissue engineering scaffolds such as collagen, agarose,[8] chitosan, or PLG.[42] Further, the combination of tissue injection molding with medical imaging is not limited to musculoskeletal tissues. The meniscus was chosen as an example of the capabilities of this technique due to its complex geometry. Given the promise demonstrated in this study, the potential exists to apply the current technique to the engineering of many tissues and organs, including cartilage, bone, skeletal muscle, cardiac muscle, and neural tissue.

ACKNOWLEDGMENTS

Alfred P. Sloan Foundation, Clark & Kirby Foundation, Soft Tissue & Sports Medicine Funds by Dr. Russell Warren, M.D., MRRCC Core Grant AR046121, Joe Lipman for technical support, and Cornell University.

REFERENCES

1. Wan, D.C., Nacamuli, R.P., and Longaker, M.T. Craniofacial bone tissue engineering. Dent Clin North Am **50,** 175, 2006.
2. Esselman, P.C., Thombs, B.D., Magyar-Russell, G., and Fauerbach, J.A. Burn rehabilitation: state of the science. Am J Phys Med Rehabil **85,** 383, 2006.
3. Jones, D.L., Westby, M.D., Greidanus, N., Johanson, N.A., Krebs, D.E., Robbins, L., Rooks, D.S., and Brander, V. Update on hip and knee arthroplasty: current state of evidence. Arthritis Rheum **53,** 772, 2005.
4. Peters, G., and Wirth, C.J. The current state of meniscal allograft transplantation and replacement. Knee **10,** 19, 2003.

5. Cao, Y., Vacanti, J.P., Paige, K.T., Upton, J., and Vacanti, C.A. Transplantation of chondrocytes utilizing a polymer–cell construct to produce tissue-engineered cartilage in the shape of a human ear. Plast Reconstr Surg **100,** 297, 1997.
6. Vacanti, C.A., Bonassar, L.J., Vacanti, M.P., and Shufflebarger, J. Replacement of an avulsed phalanx with tissue-engineered bone. N Engl J Med **344,** 1511, 2001.
7. Weng, Y., Cao, Y., Silva, C.A., Vacanti, M.P., and Vacanti, C.A. Tissue-engineered composites of bone and cartilage for mandible condylar reconstruction. J Oral Maxillofac Surg **59,** 185, 2001.
8. Hung, C.T., Lima, E.G., Mauck, R.L., Takai, E., LeRoux, M.A., Lu, H.H., Stark, R.G., Guo, X.E., and Ateshian, G.A. Anatomically shaped osteochondral constructs for articular cartilage repair. J Biomech **36,** 1853, 2003.
9. Isogai, N., Landis, W., Kim, T.H., Gerstenfeld, L.C., Upton, J., and Vacanti, J.P. Formation of phalanges and small joints by tissue-engineering. J Bone Joint Surg Am **81,** 306, 1999.
10. Rotter, N., Bonassar, L.J., Tobias, G., Lebl, M., Roy, A.K., and Vacanti, C.A. Age dependence of biochemical and biomechanical properties of tissue-engineered human septal cartilage. Biomaterials **23,** 3087, 2002.
11. Hoque, M.E., Hutmacher, D.W., Feng, W., Li, S., Huang, M.H., Vert, M., and Wong, Y.S. Fabrication using a rapid prototyping system and *in vitro* characterization of PEG–PCL–PLA scaffolds for tissue engineering. J Biomater Sci Polym Ed **16,** 1595, 2005.
12. Chang, S.C., Rowley, J.A., Tobias, G., Genes, N.G., Roy, A.K., Mooney, D.J., Vacanti, C.A., and Bonassar, L.J. Injection molding of chondrocyte/alginate constructs in the shape of facial implants. J Biomed Mater Res **55,** 503, 2001.
13. Chang, S.C., Tobias, G., Roy, A.K., Vacanti, C.A., and Bonassar, L.J. Tissue engineering of autologous cartilage for craniofacial reconstruction by injection molding. Plast Reconstr Surg **112,** 793, 2003.
14. Hott, M.E., Megerian, C.A., Beane, R., and Bonassar, L.J. Fabrication of tissue engineered tympanic membrane patches using computer-aided design and injection molding. Laryngoscope **114,** 1290, 2004.
15. Izuta, Y., Ochi, M., Adachi, N., Deie, M., Yamasaki, T., and Shinomiya, R. Meniscal repair using bone marrow-derived mesenchymal stem cells: experimental study using green fluorescent protein transgenic rats. Knee **12,** 217, 2005.
16. Reguzzoni, M., Manelli, A., Ronga, M., Raspanti, M., and Grassi, F.A. Histology and ultrastructure of a tissue-engineered collagen meniscus before and after implantation. J Biomed Mater Res B Appl Biomater **74,** 808, 2005.
17. Martinek, V., Ueblacker, P., Braun, K., Nitschke, S., Mannhardt, R., Specht, K., Gansbacher, B., and Imhoff, A.B. Second generation of meniscus transplantation: *in-vivo* study with tissue engineered meniscus replacement. Arch Orthop Trauma Surg **126,** 228, 2006.
18. Aufderheide, A.C., and Athanasiou, K.A. Comparison of scaffolds and culture conditions for tissue engineering of the knee meniscus. Tissue Eng **11,** 1095, 2005.
19. Neves, A.A., Medcalf, N., and Brindle, K.M. Influence of stirring-induced mixing on cell proliferation and extracellular matrix deposition in meniscal cartilage constructs based on polyethylene terephthalate scaffolds. Biomaterials **26,** 4828, 2005.
20. Pangborn, C.A., and Athanasiou, K.A. Growth factors and fibrochondrocytes in scaffolds. J Orthop Res **23,** 1184, 2005.
21. Kang, S.W., Son, S.M., Lee, J.S., Lee, E.S., Lee, K.Y., Park, S.G., Park, J.H., and Kim, B.S. Regeneration of whole meniscus using meniscal cells and polymer scaffolds in a rabbit total meniscectomy model. J Biomed Mater Res A **78,** 659, 2006.
22. Tienen, T.G., Heijkants, R.G., de Groot, J.H., Pennings, A.J., Schouten, A.J., Veth, R.P., and Buma, P. Replacement of the knee meniscus by a porous polymer implant: a study in dogs. Am J Sports Med **34,** 64, 2006.
23. Gleghorn, J.P., Jones, A.R., Flannery, C.R., and Bonassar, L.J. Boundary mode frictional properties of engineered cartilaginous tissue. Eur Cell Mater **14,** 20, 2007.
24. Oegema, T.R., Carpenter, B.J., and Thompson, R.C., Fluorometric determination of DNA in cartilage of various species. J Orthop Res **1,** 345, 1984.
25. Kim, Y.J., Sah, R.L., Doong, J.Y., and Grodzinsky, A.J. Fluorometric assay of DNA in cartilage explants using Hoechst 33258. Anal Biochem **174,** 168, 1988.
26. Enobakhare, B.O., Bader, D.L., and Lee, D.A. Quantification of sulfated glycosaminoglycans in chondrocyte/alginate cultures, by use of **1**,9-dimethylmethylene blue. Anal Biochem **243,** 189, 1996.
27. Neuman, R.E., and Logan, M.A. The determination of hydroxyproline. Biol Chem **184,** 299, 1949.
28. Nakamura, K., Kawaguchi, H., Aoyama, I., Hanada, K., Hiyama, Y., Awa, T., Tamura, M., and Kurokawa, T. Stimulation of bone formation by intraosseous application of recombinant basic fibroblast growth factor in normal and ovariectomized rabbits. J Orthop Res **15,** 213, 1997.
29. Almarza, A.J., and Athanasiou, K.A. Design characteristics for the tissue engineering of cartilaginous tissues. Ann Biomed Eng **32,** 2, 2004.
30. Oegema, T.R., Deloria, L.B., Sandy, J.D., and Hart, D.A. Effect of oral glucosamine on cartilage and meniscus in normal and chymopapain-injected knees of young rabbits. Arthritis Rheum **46,** 2495, 2002.
31. Sweigart, M.A., Zhu, C.F., Burt, D.M., DeHoll, P.D., Agrawal, C.M., Clanton, T.O., and Athanasiou, K.A. Intraspecies and interspecies comparison of the compressive properties of the medial meniscus. Ann Biomed Eng **32,** 1569, 2004.
32. Proctor, C.S., Schmidt, M.B., Whipple, R.R., Kelly, M.A., and Mow, V.C. Material properties of the normal medial bovine meniscus. J Orthop Res **7,** 771, 1989.
33. Perie, D.S., Maclean, J.J., Owen, J.P., and Iatridis, J.C. Correlating material properties with tissue composition in enzymatically digested bovine annulus fibrosus and nucleus pulposus tissue. Ann Biomed Eng **34,** 769, 2006.
34. Kelly, D.J., Crawford, A., Dickinson, S.C., Sims, T.J., Mundy, J., Hollander, A.P., Prendergast, P.J., and Hatton, P.V. Biochemical markers of the mechanical quality of engineered hyaline cartilage. J Mater Sci Mater Med **18,** 273, 2007.
35. Malda, J., Martens, D.E., Tramper, J., van Blitterswijk, C.A., and Riesle, J. Cartilage tissue engineering: controversy in the effect of oxygen. Crit Rev Biotechnol **23,** 175, 2003.
36. Adesida, A.B., Grady, L.M., Khan, W.S., and Hardingham, T.E. The matrix-forming phenotype of cultured human meniscus cells is enhanced after culture with fibroblast growth factor 2 and is further stimulated by hypoxia. Arthritis Res Ther **8,** R61, 2006.

37. Basser, P.J., and Pajevic, S. A normal distribution for tensor-valued random variables: applications to diffusion tensor MRI. IEEE Trans Med Imaging **22,** 785, 2003.
38. Palmer, A.W., Guldberg, R.E., and Levenston, M.E. Analysis of cartilage matrix fixed charged density and threedimensional morphology via contrast-enhanced microcomputer tomography. Proc Natl Acad Sci USA **103,** 19255, 2006.
39. Dienst, M., Greis, P.E., Ellis, B.J., Bachus, K.N., and Burks, R.T. Effect of lateral meniscal allograft sizing on contact mechanics of the lateral tibial platean experimental study in human cadaveric knee joints. Am J Sports Med **35,** 34, 2007.
40. Huang, A., Hull, M.L., Howell, S.M., and Haut Donahue, T. Identification of cross-sectional parameters of lateral meniscal allografts that predict tibial contact pressure in human cadaveric knees. J Biomech Eng **124,** 481, 2002.
41. Donahue, T.L., Hull, M.L., and Howell, S.M. New algorithm for selecting meniscal allografts that best match the size and shape of the damaged meniscus. J Orthop Res **24,** 1535, 2006.
42. Mercier, N.R., Costantino, H.R., Tracy, M.A., and Bonassar, L.J. Poly(lactide-*co*-glycolide) microspheres as a moldable scaffold for cartilage tissue engineering. Biomaterials **26,** 1945, 2005.

Address reprint requests to:
Lawrence J. Bonassar, Ph.D.
Cornell University
218 Upson Hall
Ithaca, NY 14853

E-mail: LB244@cornell.edu

Received: June 28, 2007
Accepted: January 14, 2008